Rhythmic Nuclear Import Mediated by Importins Regulates the *Neurospora* Circadian Clock.

Ziyan Wang[a], Bin Wang[a], Bradley M. Bartholomai[a], Jennifer J. Loros[b], Jay C. Dunlap[a+]

[a] Department of Molecular and Systems Biology, [b] Department of Biochemistry and Cell Biology, Geisel School of Medicine at Dartmouth, Hanover, NH, USA

[+]Corresponding author: J. C. Dunlap, jay.c.dunlap@dartmouth.edu

Key words: FREQUENCY (FRQ), White Collar Complex (WCC), Fluorescent live-cell imaging, nucleocytoplasmic transportation, FRAP, fungi

ABSTRACT

Circadian clocks in eukaryotes rely on precisely regulated negative feedback loops to generate daily rhythms. However, the delay mechanisms that extend this structurally simple feedback loop to ~24 hours are not yet fully understood. In the filamentous fungal model organism *Neurospora crassa*, the negative arm complex, centered by FREQUENCY (FRQ), must enter the nucleus to repress the White Collar Complex (WCC) and close the feedback loop, but the mechanisms and dynamics of its nuclear transport have remained unresolved. Using long-term live-cell imaging and fluorescence recovery after photobleaching (FRAP), we demonstrate that FRQ nuclear import is an active circadian-regulated process that is fastest early in the subjective day and progressively decreases as nuclear FRQ approaches peak levels, corresponding to altered direct binding between FRQ and Importin α. We further establish that Importin α is required for the spatial regulation of FRQ and WC-1 and the correct timing of *Neurospora* circadian clock. Analysis of the three *Neurospora* Importin β homologs reveals that each of them contributes differently to the circadian clock through pathways beyond FRQ or WCC nuclear import. More specifically, we find a genetic interaction between Impβ3 and the phosphatase PP-4. Together, these findings indicate that nuclear import is a selective, dynamic, and rate-limiting regulatory step in the fungal circadian clock and reveal both conserved and fungal-specific mechanisms by which importins tune circadian timing.

INTRODUCTION

Circadian clocks are self-sustained timekeeping systems that allow organisms to anticipate and adapt to daily changes in the environment. These oscillators are based on conserved transcription-translation feedback loops (TTFLs) in which the Positive Arm (typically transcription factors) drives expression of the Negative Arm that, once translated and imported into nuclei, inhibit its own activators (Dunlap, 1999; Hardin, 2011; Partch et al., 2014). A key feature of this design is that multiple built-in delays extend the simple feedback loop to maintain a ~24-hour periodicity that approximates environmental changes.

Precisely timed nuclear entry of Negative Arm components can act as a rate-limiting step that introduces phase delay between transcriptional activation and repression. Importins (karyopherins) mediate the nucleocytoplasmic transport of most proteins through the nuclear pore complex (NPC) (Chook and Blobel 2001; Pemberton and Paschal 2005). There are two major nuclear import pathways: the classical Importin α (Impα)-dependent pathway, in which Impα, as an adaptor, binds cargos with canonical nuclear localization signals (NLSs) and delivers them to Importin β (Impβ); and the Impα-independent pathway, in which Impβ directly recognizes non-classical NLSs. In *Drosophila*, the clock protein dTIM binds directly to Impα1 and co-transports dPER, and perturbations of Impα1 alter circadian period and rhythmicity (Jang et al. 2015; Lin et al. 2023). In mammals, the extent to which nuclear import of PERs and CRYs requires Impα remains debatable and may rely more directly on Impβ family members. In human cells, KPNB1 (Impβ1) mediates nuclear import of some PER/CRY complexes independently of Impα (KPNA1/2), and TNPO1 (Impβ2) selectively regulates PER1 localization and period length (Lee et al. 2015; Korge et al. 2018; Lee et al. 2019). However, chemical inhibition of the classical Impα/β1 pathway also alters period length (Öllinger et al. 2014), and in mouse, nuclear import of mCRY2 is Impα-dependent (Sakakida et al. 2005). These findings suggest that controlled nuclear entry of the Negative Arm is a conserved step important for circadian timing, but the exact pathways and molecular players differ: Impα is essential in *Drosophila*, while in mammals PER and CRY can sometimes bypass Impα and depend on specific Impβs. In contrast to animal circadian systems, little is known about how the Positive and Negative Arm components of fungal clocks such as *Neurospora* enter the nucleus.

The filamentous fungus *Neurospora crassa* has been a powerful model for studying circadian clocks. The Positive Arm of its oscillator is the White Collar Complex (WCC, a heterodimer of WC-1 and WC-2), which activates transcription of the *frequency* (*frq* gene) whose product serves to nucleate the Negative Arm complex of FRQ, FRH, and CK1. This complex then feeds back to repress WCC activity (Crosthwaite et al. 1997; Dunlap 1999; Dunlap and Loros 2017; Costa et al. 2025). FRQ is highly concentrated in the nucleus, which makes sense because its nuclear entry is required for inhibitory function on WCC and is essential for closing the negative feedback loop (Wang et al. 2025). Thus, FRQ nuclear transport is a central regulatory point in the *Neurospora* clock.

Despite its importance, the mechanism of FRQ nuclear transport remains unclear. An NLS within FRQ was reported more than two decades ago and suggested to be essential for both nuclear localization and clock function (Luo et al. 1998), but this has not been thoroughly tested with modern tools, and the transport machinery has also not been defined. Unlike animals,

which express three classes of Importin α subunits (e.g. six in human genome) with overlapping and specialized functions, plants and fungi only have one class of Importin α that resembles animal α1(Goldfarb et al. 2004; Mason et al. 2009; Bernardes et al. 2020). Within the fungal kingdom, nuclear import pathways have only been systematically studied in yeast and *Aspergillus nidulans*. A few related studies in *Neurospora* focused on the conserved structure and epigenetic function of Impα (Takeda et al. 2013; Bernardes et al. 2015; Klocko et al. 2015). Through identification of homologs using NCBI orthologs based on the Karyopherin-β family in *Saccharomyces cerevisiae* and *Aspergillus nidulans* (Ström and Weis 2001; Mans et al. 2004; Markina-Iñarrairaegui et al. 2011), we identified a single Impα, three Impβs and nine other potential Karyopherins including Exportin-1 in *Neurospora crassa* (Supplementary Table 1). Mass spectrometry studies suggested FRQ may weakly interact with Impα and/or Impβ3 (Baker 2010; Pelham et al. 2023), but biochemical, functional and biological validation is lacking. How these Importins contribute to FRQ nuclear entry or to subcellular localization of other clock proteins is unknown. In part this is due to technical challenges which have further limited progress. The insufficient brightness of FRQ-GFP fusion protein prevented reliable imaging, and an “anchor-away” assay (Haruki et al. 2008), which used FRQ fused to FRB artificially tethered to FKBP-tagged histone H1 to assay nuclear import, introduced non-physiological import routes and disrupted normal clock function (Diernfellner et al., 2009). As a result, the dynamics and regulation of FRQ nuclear transport in *Neurospora* remain poorly characterized.

In this study, we used live-cell imaging combined with FRAP to directly measure FRQ nuclear import in *Neurospora*. We found that FRQ is imported slowly, requiring tens of minutes for recovery, and that import is strongly regulated across the circadian cycle, being highest early in the subjective day and reduced near nuclear peak levels. These dynamics are comparable to those of mammalian PER proteins, suggesting that slow nuclear import is a conserved delay mechanism in circadian clocks. We further show that FRQ import requires importin α but not the previously proposed NLS, and that import of WC-1, but not WC-2, also depends on importin α. Finally, we find that the three importin βs have distinct contributions to circadian regulation, including a potential link between Impβ3 and PPH-4. Together, these results reveal nuclear import as a selective and regulated process that is essential for circadian timing in *Neurospora*.

RESULTS

Nuclear import rate of FRQ is circadianly regulated.

Precisely timed nuclear localization of FRQ is essential for the normal operation of the circadian clock. To understand how and when FRQ enters nuclei, we optimized FRAP experiments for *Neurospora* building on the continuous live-cell imaging approach reported separately (Wang et al. 2025). An imaging strain blind to blue light carrying endogenously mNeonGreen-tagged FRQ (strain 1952-2; *his-3::frq*$_{cbox}$*-luc; ras-1*^{bd}*; wc-1*$^{\Delta LOV}$*, for, frq*^{mNeonGreen_Flag}) retains an intact circadian clock (Fig. S1A-C). The application of microfluidic devices allows convenient medium exchange, enabling application of the microtubule inhibitor benomyl at specific times. Benomyl slows nuclear movement by disrupting active transport along microtubules and by reducing growth, which decreases passive movement driven by bulk cytoplasmic flow and thereby facilitating imaging. Importantly, benomyl does not affect circadian functions (Fig. S1D). For FRAP experiments, a thick optical section (around 2 μm, corresponding to the diameter of *Neurospora* nuclei) was chosen to minimize artifacts from vertical random movement of nuclei. Cultures in microfluidic devices (Wang et al. 2025) were entrained with 12h:12h temperature cycles mimicking natural conditions, and FRAP was then performed every 30 minutes during the subjective day on the same culture (Fig.1A). After bleaching entire target nuclei, the subsequent recovery of fluorescence reflects import of unbleached cytoplasmic FRQ^{mNG} at that time.

The nuclear fluorescence from FRQ^{mNeonGreen} recovered most rapidly early in the subjective day, indicating a higher import rate, while the recovery was slower later in the subjective day (Fig. 1B-C, Supplementary Video 1). This temporal difference is consistent with the progressive nuclear accumulation of FRQ during the subjective day that we observed previously (Wang et al. 2025). Near subjective dawn, the recovered signal could even exceed the pre-bleaching level (e.g. 129 ± 29% at 23 minutes post-bleaching at CT3). By contrast, at subjective dusk, when nuclear FRQ levels reach their peak, nuclear import was remarkably reduced (Fig. 1C-D).

Due to the slow FRQ import rate we observed, most recovery curves failed to reach a stable plateau within the 25-minute observation window. To ensure consistent analyses, we used linear regression rather than the commonly used exponential fit to calculate nuclear import rates. To compensate for high variability in nuclear movements and possible artifacts, multiple control nuclei within each culture were averaged and used to correct for unavoidable photobleaching caused by continuously imaging. The nuclear import rate shows a significant negative correlation with time during the subjective day (Fig. 1D, Fig. S1E). Consistent results were observed when using a single corresponding nucleus from the same experiment, without averaging (Fig. S1F). In conclusion, nuclear import rates of FRQ are circadian regulated with a peak in the subjective morning.

FRQ is transported into nuclei through the Impα import pathway.

Because previous mass spectrometry had identified Impα as a possible weak interactor of FRQ (Baker et al. 2009; Baker 2010), we hypothesized that the time-dependent regulation of FRQ nuclear import is mediated by its interaction with importin α (Impα). To verify this interaction, we endogenously tagged Impα with the V5 epitope tag at its C-terminus. Co-immunoprecipitation with V5 beads successfully enriched Impα^{V5}, and FRQ co-precipitated with Impα^{V5} at early time

142 points, corresponding to times showing rapid nuclear import (Fig. 2A, Fig, S2A-B). However, at
143 later time points when FRQ is more abundant, binding between FRQ and Impα^{V5} is barely
144 detectable, corresponding to times of slower import. The change in binding strength is
145 consistent with this being the cause for precisely controlled nuclear import.

146 Impα is expected to act through nuclear localization signals (NLS) (Conti et al. 1998; Takeda et
147 al. 2013). Several putative NLS have been suggested on FRQ, with one of them being essential
148 to circadian clock (Luo et al. 1998). We reconstituted Neurospora strains bearing FRQ at its
149 endogenous locus with the FRQ-NLS deleted, with or without the mNeonGreen tag to allow for
150 fluorescent imaging, to directly assess the contribution of the predicted NLS to FRQ nuclear
151 entry. The reconstituted strains recapitulate the arrhythmic phenotype as expected (Fig. S2C).
152 To delineate nuclear boundaries, two nuclear envelope proteins, Nup159 (NCU08604) in the
153 cytoplasmic side of nuclear pore complexes and Nup211 (NCU04059) in the nuclear basket
154 complexes, were tagged at their endogenous loci using different fluorescent tags to serve as
155 markers for the outer and inner sides of the nuclear membrane, respectively (Beck and Hurt
156 2017; Bartholomai 2022). Both proteins form fragmented ring-like structures that largely align
157 with each other at the nuclear periphery, with the two layers clearly distinguishable when
158 imaged on SoRa super-resolution microscope (Fig. S2D). To our surprise, although rhythmicity
159 was plainly diminished (Fig. S2C), FRQ still localized to nuclei and nuclear FRQ levels remained
160 constantly high when the proposed NLS is absent (Fig. 2B-C, Fig, S2E). This nuclear
161 localization is not an artifact caused by mNeonGreen tagging, as other tagged *Neurospora*
162 proteins, like the septin CDC-11, localized to cytoplasm as expected (Fig. S2F). Nuclear FRQ
163 still forms highly dynamic nuclear bodies in the *frq*$^{\Delta NLS}$ strain, with subnuclear heterogeneity
164 levels indistinguishable from that of wildtype FRQ (Fig. S2G, Supplementary Video 2)

165 Impα plays an important role in *Neurospora* development and growth (Klocko et al. 2015) and
166 complete depletion of Impα is lethal. To assess the functional role of Impα, we used an RNAi
167 approach to knock down *impa* under the control of a quinic acid (QA)-inducible promoter (Giles
168 et al. 1985; Shi et al. 2010) (Fig. 3A). Addition of QA leads to severe growth defects (Fig. 3B),
169 and short induction (20 hours) is sufficient to significantly reduce both *impa* transcript and Impα
170 protein levels, while not causing macroscopical sickness or death (Fig. 3C-D). Due to leakiness
171 of the *qa-2* promoter (Larrondo et al. 2009), some reduction of Impα was also observed in the
172 inducible RNAi strains even without induction (Fig. 3C-D, Fig, S3A). The progressive decrease
173 in Impα levels, from the no-dsRNA control strain (*impα*^{V5}) to inducible RNAi strains without QA,
174 and finally to the inducible RNAi strains with QA, provided a platform to assay dose-dependent
175 circadian phenotypes caused by Impα deficiency.

176 We examined circadian rhythms in Impα knockdown strains using the luciferase reporter driven
177 by the *frq*$_{cbox}$ promoter described above. Control cultures exhibited ~22 h rhythms, whereas
178 progressive depletion of Impα shortened the period and stronger knockdown abolished
179 rhythmicity, resulting in arrhythmic or inviable cultures (Fig. 3E, Fig. S3B). Indeed, cultures
180 displayed sensitivity to extremely low levels of inhibition, comparing reductions seen in Fig. 3C-
181 D with rhythm phenotypes in Fig. 3E. Another striking effect caused by Impα deficiency is that
182 all tested core clock proteins, as well as non-clock-related protein Tubulin, decrease in bulk
183 tissues collected from liquid cultures (Fig. 3D). In contrast, the most abundant proteins that

184 dominate unspecific protein measurements remain unchanged. This may reflect a reduction in
185 metabolically active tissue due to sickness in Impα-deficient culture, while the structural
186 components in older tissue remain largely intact.

187 Live-cell fluorescent imaging allows dissection of local changes in metabolically active tissue,
188 such as the actively growing tip regions. These results are consistent with biochemical
189 analyses, showing that with Impα knocked down, FRQ nuclear import was clearly impaired (Fig.
190 4A). In the control strains, addition of QA (which also provides an extra nutrient source) boosts
191 nuclear FRQ levels (Fig. 4A-C, Fig. S3C). In contrast, in the RNAi strains, QA addition caused
192 reduced or unchanged nuclear FRQ, compared to the increase in the control strain, despite total
193 FRQ levels in the tip region remaining relatively constant (Fig. 4A-C, Fig. S3C). This indicates
194 that without sufficient Impα, FRQ accumulates in the cytoplasm and fails to efficiently enter
195 nuclei to shut down its own synthesis. Even in the absence of QA, the leaky knockdown of Impα
196 resulted in a mild reduction in nuclear FRQ compared to controls (Fig. 2B). Together, these
197 observations support the model that FRQ nuclear import is actively mediated by the Impα
198 pathway and is regulated across the circadian cycle to ensure appropriate timing and rates of
199 nuclear entry, both of which are essential for maintaining circadian stability.

200 **WC-1 but not WC-2 also depends on Impα for nuclear import.**

201 The most obvious change in clock protein levels is that WC-1 becomes undetectable by western
202 blot with severe deficiency of Impα (Fig. 3D), even though the expression level of *wc-1*
203 transcripts is unchanged (Fig. 3C). This divergence indicates that the defect occurs at the post-
204 transcriptional level, either through impaired translation or reduced WC-1 protein stability.
205 Interestingly, WC-1 co-immunoprecipitates with Impα in a phase-dependent manner (Fig. 2A),
206 similar to FRQ. Because WC-1 is predominantly found in the nucleus, this suggests a model in
207 which WC-1 is unstable in the cytoplasm. When nuclear import of WC-1 is blocked by deficiency
208 of Impα, newly synthesized WC-1 is trapped in cytoplasm, being unstable, and is rapidly
209 degraded (Fig. 4D).

210 Although rhythmic turnover of WCC is not essential for circadian clock regulation, the presence
211 of nuclear WC-1 is essential. While WC-1 is below the detection limit of western blotting in Impα
212 knockdown strains (Fig. S3A), a trace amount of WC-1 may still be able to support circadian
213 function (Lee et al. 2003; Káldi et al. 2006). Consistent with this, the expression of its direct
214 target *frq* is unaffected (Fig. 3C). The photoreceptor function of WC-1 is intact as well; both *wc-1*
215 and *frq* transcript levels increase drastically after a 15-minute light pulse (Fig. 4E-F).
216 Surprisingly, *impα* itself also turns out to be light-inducible (Fig. 4G), although it was not
217 previously identified as a light responsive gene by RNA-seq (Chen et al. 2009; Smith et al.
218 2010; Dekhang et al. 2017). Even though the residual WC-1 retains functions when Impα is
219 reduced, its overall efficiency is compromised, as the fold increase of gene expression in
220 response to light is smaller compared to no QA (Fig. S3D). In this context, it may be that less
221 FRQ is needed to fully inhibit the limited WCC activity during circadian cycles, which may
222 explain the observed period shortening despite slow FRQ nuclear import.

223 WC-2 also co-precipitated with Impα in a phase-dependent manner (Fig. 2A). However, both
224 nuclear and total levels of WC-2 in tip regions increase significantly as the level of Impα

225 decreases (Fig. 4A, H-I, Fig. S3E). Overall, the nuclear import of WC-2 does not appear to rely
226 on the Impα pathway. The observed co-immunoprecipitation is likely mediated through WC-2's
227 association with WC-1, and may not reflect a direct or biologically relevant interaction.

228 **Deficiency of importin βs have divergent effects on circadian clock.**

229 The genes encoding the three identified Impβ subunits in *Neurospora crassa* are NCU02011,
230 NCU03690, and NCU02357 (Supplementary Table 1) (Galagan et al. 2003). Homologs of two of
231 the three Impβs, Impβ1 (NCU02011; mammalian KPNB1) and Impβ2 (NCU03690; mammalian
232 TNPO1), have been associated with nuclear import of Negative Arm components PER1 and
233 PER2 in mammalian systems (Lee et al. 2015; Korge et al. 2018; Lee et al. 2019). Impβ3
234 (NCU02357; mammalian IPO5) has not been linked to circadian regulation in any system, but
235 was identified as a potential FRQ interactor at DD24 by mass spectrometry (Pelham et al.
236 2023). We therefore investigated how deficiency of these three Impβs affect circadian clock
237 using different strategies.

238 *impβ1* is an essential gene - neither homozygous knockouts nor inducible *impβ1* strains (with
239 *impβ1* expression driven by either *qa-2* or *tcu-1* promoters) are viable. Moreover, RNAi targeting
240 of two distinct regions of the *impβ1* gene, using the same strategy applied to *impα*, failed to
241 cause a strong growth defect and at best only reduced the expression level by around 40% (Fig.
242 S4A). As an alternative approach to achieve deficiency of Impβ1, we tested two Impβ1
243 inhibitors, Importazole and Ivermectin (Soderholm et al. 2011; Wagstaff et al. 2011). Both drugs
244 cause growth defects, with Importazole having less severe effects in a dose-dependent manner
245 (Fig. S4B). Based on the growth tests, 40μM drugs were used for fluorescent imaging
246 experiments. Importazole inhibits FRQ nuclear localization (Fig. 5A-C), suggesting a potential
247 role of Impβ1 in nuclear import, possibly together with Impα. Ivermectin treatment instead leads
248 to an overall increase in hyphal fluorescence without changing in nuclear signal (Fig. S4C-E),
249 which could result from cytoplasmic accumulation of FRQ or increased autofluorescence due to
250 growth-associated stress.

251 A full knockout of *impβ2* causes minor growth defects (Fig. S4F), shortens circadian period by
252 around 2.5 hours, and slightly reduces WCC activity leading to loss of persistence of the rhythm
253 (Fig. 5D-E). Consistent with this, knockdown or knockout of TNPO1 in mammalian cells also
254 shortens circadian period (Korge et al. 2018), suggesting a similar regulatory mechanism
255 between the two circadian systems. However, nuclear localization of neither FRQ nor WC-2 is
256 impaired in the *Δimpβ* knockout strains (Fig. 5F-G). FRAP experiments at CT4 showed no
257 difference in FRQ nuclear import rate either (Fig. 5H). There are also no obvious changes in
258 core clock protein expression levels in the *Δimpβ* knockout strains (Fig. S4G).

259 *impβ3* is also essential, but viable conditional knockdowns were achieved by insertion of the
260 inducible *qa-2* promoter directly upstream of the ORF (Fig. 6A). A VHF tag was fused to its C
261 terminus to facilitate protein detection. In the absence of QA, the expression level of Impβ3 is
262 significantly decreased (Fig. 6B, Fig. S5A), resulting in a substantial circadian period length
263 shortening to around 15 hours. A relatively small amount of Impβ3 is sufficient to sustain a
264 normal clock, as even a low concentration (10^{-4}M) of QA restores the period to wild-type length,
265 and higher QA concentrations have no additional effect (Fig. 6C, Fig. S5B-C). Expression of

266 core clock proteins remains normal in Impβ3-deficient samples (Fig. 6B, Fig. S5A). To examine
267 subcellular localization of core clock components, endogenous fluorescent-tagged *frq* or *wc-2*
268 alleles were introduced into the inducible strain, which exhibited dramatically shortened periods
269 as expected (Fig. S5D). Despite the period effects, loss of Impβ3 resulted in no reduction in
270 nuclear localization of either FRQ or WC-2 (Fig. 6D-E).

271 Period shortening, particularly the dramatic period shortening seen with reduced Impβ3, is less
272 often seen with clock mutants. This prompted us to further investigate the possible mechanism
273 by which Impβ3 regulates the circadian clock by looking for possible interactions with protein
274 phosphatase 4 (PP4) whose loss also results in period shortening. PP4 has previously been
275 shown to regulate the nuclear enrichment of the WCC, and loss of *pph-4* also results in a
276 shortened circadian period, similarly to Impβ3 knockdown (Fig. S5E) (Cha et al. 2008; Dasgupta
277 2015). Interestingly, the period phenotypes caused *Δpph4* and *impβ3* reduction are not additive;
278 that is, knockdown on *impβ3* is epistatic to *pph4*. When Impβ3 is present (with QA), *Δpph-4*
279 caused the expected period shortening (Fig. S5E). However, using the same pair of strains,
280 combining *Δpph-4* with Impβ3 reduction (no QA) does not further shorten the circadian period
281 although rhythm persistence is reduced (Fig. 6F, Fig. S5E). This non-additive effect suggests
282 that Impβ3 and PP4 act within the same or overlapping pathways to regulate circadian
283 rhythmicity. Impβ3 may facilitate the proper subcellular localization of PP4 or its associated co-
284 enzymes, thereby enabling PP4 to precisely regulate phosphorylations of core clock proteins.
285 These findings point to functional crosstalk between nucleocytoplasmic transportation and
286 phosphatase-mediated regulation in maintaining the accuracy of circadian clock.

DISCUSSION

Our findings establish nuclear import as a key regulatory step in the *Neurospora* circadian clock. Using the live-cell imaging platform (Wang et al. 2025), we are able to measure in vivo subcellular dynamics in *N. crassa* under native, biologically relevant conditions. Through FRAP, we observed that FRQ is imported into nuclei slowly during the subjective day, requiring >20 min to recover fluorescence (Fig. 1). This disagrees with an earlier report of rapid nucleocytoplasmic shuttling of FRQ based on an anchor-away strategy that fused FRQ to FRB and tethered it to FKBP-tagged histone H1 (Diernfellner et al., 2009). While powerful, that system relies on rapamycin-induced heterodimerization of FRB-FKBP, which introduces an artificial import route that could diminish intrinsic clock function, raising the possibility that the observed fast shuttling is a result of methodological differences rather than the intrinsic behavior of FRQ in a free-running circadian cycle.

FRAP analyses revealed that FRQ nuclear import is not constant but varies across different stages of FRQ nuclear accumulation of the circadian cycle, being most active early in the subjective day and strongly weakened near subjective dusk (Fig. 1). This temporal regulation ensures that nuclear FRQ accumulation occurs with proper timing and rate, contributing to period stability. A previous report using FRAP to estimate nuclear import of mammalian Negative Arm proteins tested only extreme time points - when nuclear levels were at their peak or trough (Smyllie et al. 2016). As these conditions represent equilibrium states with little net nucleocytoplasmic exchange, it may be reasonable that no difference in import rate was detected (Smyllie et al. 2016). In contrast, by assaying import continuously across the subjective day, we observed a gradual decrease in nuclear import as FRQ approached its peak nuclear accumulation. The timescale of FRQ import we observed by FRAP (tens of minutes for recovery) is comparable to that of PER1 and PER2, functional homologs of FRQ in mammalian systems, whether assayed through endogenous tagging or transient expression (Öllinger et al. 2014; Smyllie et al. 2016; Korge et al. 2018). This similarity across fungal and mammalian systems suggests that slow nuclear import is a conserved feature of Negative Arm proteins and may represent an important delay step required to sustain a ~24-hour feedback loop.

Impα has been shown to regulate the subcellular localization of the Negative Arm in both mammalian systems and *Drosophila* (Umemura et al. 2014; Jang et al. 2015). The dependence of FRQ nuclear import on Impα, supported by both biochemical Co-IP and fluorescent imaging after RNAi knockdown experiments, places Impα at the core of this regulatory process (Fig. 2-4). Impα facilitates nuclear import by directly binding to the NLS on a target protein (Conti et al. 1998). Surprisingly, a domain previously shown to be essential for circadian rhythmicity suggested to function as a NLS on FRQ (Luo et al. 1998), is not required for nuclear localization of FRQ (Fig. 2) (Schunke et al. 2025). These strains exhibit persistently high WCC activity, suggesting that the loss of rhythmicity arises from a failure of FRQ to inhibit WCC despite its nuclear presence. Deletion of this motif has also been proposed to disrupt FRQ dimerization (Lauinger et al. 2014), which is essential for circadian clock and could be the cause of arrhythmicity (Cheng et al. 2001). A very recent work overexpressing fluorescent tagged FRQ fragments in mammalian cell culture support our conclusion and suggest the possible presence of multiple redundant NLSs on FRQ (Schunke et al. 2025). Similar redundancy has also been

329 reported for the Positive Arm WCC, whose nuclear localization doesn't rely on a single NLS
330 (Schwerdtfeger and Linden 2000; Cheng et al. 2003; Wang et al. 2016). Together, these
331 observations suggest that nuclear import in *Neurospora* is governed by a more complex and
332 possibly redundant regulatory mechanism than seen in other eukaryotes (Sakakida et al. 2005;
333 Kwon et al. 2006; Saez et al. 2011), consistent with the unique challenges posed by its syncytial
334 organization.

335 In addition to FRQ, our results demonstrate that WC-1 nuclear import is also strongly dependent
336 on Impα (Fig. 3-4). In Impα-deficient strains, WC-1 protein became undetectable despite normal
337 transcript levels, consistent with post-transcriptional destabilization. It may be that WC-1 is
338 unstable in the cytoplasm and is rapidly degraded when nuclear import is blocked, thereby
339 explaining the dramatic loss of WC-1 protein in Impα-deficient strains. By contrast, WC-2
340 nuclear import does not require Impα and its nuclear localization even increases with reduced
341 Impα. Although the overall amount of nuclear WCC does not show strong oscillations (Denault
342 et al. 2001), WCC has been reported to undergo rapid nucleocytoplasmic shuttling (Schafmeier
343 et al. 2008). NCU01249 encodes the sole Impα subunit in *Neurospora*, which must control
344 nuclear import of numerous cargo proteins and has been linked to additional cellular functions
345 beyond nuclear import (Klocko et al. 2015). Therefore, the effects of Impα deficiency on both
346 growth and circadian rhythmicity is likely mediated through multiple pathways beyond altered
347 localization of core clock proteins.

348 Our analysis of Impβ proteins further underscores the complexity of importin-mediated
349 regulation (Fig. 5-6). Impβ1 is essential and difficult to genetically manipulate, but chemical
350 inhibition suggests a role in FRQ nuclear localization, possibly in cooperation with Impα. Impβ2
351 deletion shortened the circadian period by ~2.5 h, paralleling results from knockdowns of its
352 mammalian homolog TNPO1 (Korge et al. 2018). However, nuclear localization of FRQ and
353 WC-2 was unaffected, suggesting that Impβ2 influences the clock through other cargoes or
354 regulatory pathways. Impβ3 is also important for precise circadian control: reduced expression
355 caused dramatic period shortening without altering nuclear localization of FRQ or WC-2, again
356 suggesting other cargoes or regulatory pathways. Genetic interaction experiments with *pph-4*
357 indicate that Impβ3 and PPH4 act within the same regulatory pathway, with Impβ3 potentially
358 functioning upstream to facilitate PPH4 activity or localization. This unexpected connection
359 highlights the interplay between nuclear transport and phosphatase-mediated regulation of
360 WCC.

361 Together, these results demonstrate that nuclear import is a dynamic and selective process that
362 plays a critical role in shaping circadian timing in *Neurospora*. Our findings parallel observations
363 in other eukaryotic systems (Sakakida et al. 2005; Saez et al. 2011; Öllinger et al. 2014;
364 Umemura et al. 2014; Jang et al. 2015; Lee et al. 2015; Korge et al. 2018; Korge et al. 2018),
365 underscoring the evolutionary conservation of importin-mediated circadian regulation, while also
366 revealing unique fungal-specific mechanisms.

367

MATERIALS AND METHODS

Strain construction:

Plasmids were constructed using pRS426 as backbone. Gene fragments were amplified from genomic DNA of *N. crassa* 74-OR23-1VA (FGSC, 2489) using Phusion Flash High-Fidelity PCR Master Mix (Thermo Scientific # F548S). Other fragments were either ordered as a gBlock or amplified from previously plasmids from the lab. Fragments were then assembled together using NEBuilder® HiFi DNA Assembly Master Mix (New England Biolabs Cat. #E2621) according to the manufacturer's instructions. All plasmids and their sequence data have been deposited at Addgene.

Plasmid	Addgene ID	Corresponding allele	Source or reference
frq[mNG_Flag]_hph	245515	*frq*^{mNeonGreen_Flag}*::hph+*	(Wang et al. 2025)
wc-2[mAp]_hph	245516	*wc-2*^{mApple}*::hph+*	
frq[ΔNLS, mNG_V5]_nat-1	251399	*frq*$^{\Delta NLS,\ mNeonGreen_V5}$*::nat-1+*	This Study
nup159[mApple]_bar	251400	*nup159*^{mApple}*::bar+*	
nup211[mTagBFP2]_hph	251401	*nup211*^{mTagBFP2}*::hph+*	
csr-1_qa-2_dsimpα_bar	251402	*csr-1::qa_dsimpα*	
wc-1[ΔLOV, mAp]_bar	251403	*wc-1*$^{\Delta LOV,\ mAp}$*::bar+*	
qa-2_[VHF]impβ3_bar	251404	*qa-2_*^{VHF}*impβ3::bar+*	
qa-2_[VHF]impβ3_nat-1	251405	*qa-2_*^{VHF}*impβ3::nat-1+*	

frq$^{\Delta NLS,\ mNeonGreen_V5}$*::nat-1+* contains the full *frq* gene with NLS1 (Luo et al. 1998) deleted, fused at its C-terminus to codon-optimized mNeonGreen and a V5 tag, followed by the nourseothricin resistance marker (He et al. 2020), designed to target the endogenous *frq* locus. The transformation cassette was amplified using Phusion Flash High-Fidelity PCR Master Mix (Thermo Scientific # F548S) and then transformed into strain 576-4 (*Δmus-52::hph+; Δfrq::hph+*).

nup159 (NCU08604) and *nup211* (NCU04059) were endogenously tagged at their C-termini using similar strategy as described previously (Bartholomai 2022) using different fluorescent tags and drug selection markers. *impα* (NCU01249) was endogenously V5-tagged at its C-terminus using a hygromycin resistant cassette for selection, resulting in the *impα*^{V5}*::hph+* allele.

The expression cassette producing double-stranded RNA targeting exon 3 of *importin α* (NCU01249) under control of the QA-inducible promoter was constructed as shown in Fig. 3A and inserted at the *csr-1* locus.

The *qa-2* promoter, along with a V5_6xHis_3xFlag (VHF) tag, was inserted at the N-terminus of *importin β3* (NCU03257) coding sequence using standard lab protocols to regulate its expression (Aronson et al. 1994). Two series of strains with different drug selection markers were constructed to accompany with other alleles during sexual crosses.

Transformations of *Neurospora crassa* were performed following lab protocol as described previously (Bartholomai 2022), after which sexual crosses were carried out using standard Neurospora methods (http://www.fgsc.net/Neurospora/NeurosporaProtocolGuide.htm) to generate homokaryotic progeny with the desired combination of alleles.

FRAP:
5 independent runs were performed for FRAP experiments using strain 1946-1 (*csr-1::son-1^{mTagBFP2}; ras-1^{bd}; wc-1$^{\Delta LOV}$::bar+, for, frq^{mNeonGreen_Flag}::hph+*) in the customized microfluidic devices as described previously (Wang et al. 2025) with Bird medium (Metzenberg 2004) containing 0.2% glucose, 0.2% poly-acrylic acid, and 1mM sodium formate. The cultures were entrained by temperature steps before resetting to CT0. 2.5 µg/ml benomyl was added to the medium at the same time of resetting. For each independent run, one FRAP experiment was performed on a new region within the same culture every half an hour from CT2 to CT10. Single focal plane images were acquired on LSM 880 with the pinhole size adjusted to an optical section of 2.8 µm. For each recording, 40 to 50 frames were collected at 30 seconds interval. After the first two frames, 4-7 nuclei were photobleached with a 488 nm laser to around 30% of the initial fluorescence intensity. SON-1^{mTagBFP2} (DAPI channel) was recorded at the same time as nuclear marker.

Measurements of F_ROI (manually bleached nuclei), P_ROI (untreated nuclei) and B_ROI (outside of the cell) were taken in ImageJ. Rolling averages of 3 time points (n-1, n, n+1) were calculated and used for further analysis. Fluorescence recordings were corrected for background. The fitted values based on an averaged slope (photobleaching rate) calculated from the linear regressions of *P_ROI - B_ROI* within the same run were used to correct for photobleaching during recording:

$$F_ROI_{corrected} = \frac{(F_ROI - B_ROI)}{(\widehat{P_ROI - B_ROI})}$$

$F_ROI_{corrected}$ was then normalized to pre-beach intensities (set as 100%) and grouped into 1-hour bins, i.e. all $F_ROI_{corrected}$ from HT3 and HT3.5 were considered as group HT3, for Fig. 1D.

A linear regression was calculated for each nucleus ($F_ROI_{corrected}$). Then, the slopes of these fitted curves were grouped into 1-hour bins for Fig. 1E. A small number of nuclei were excluded because of poor goodness of fit (r^2).

Time	CT2	CT3	CT4	CT5	CT6	CT7	CT8	CT9	CT10
N of included nuclei ($r^2 \geqslant 0.5$)	4	22	26	32	35	37	32	24	18
N of excluded nuclei ($r^2 < 0.5$)	0	1	1	1	0	1	1	2	0

For Fig. S1E, a similar analysis was performed using linear regression of a single example *P_ROI - B_ROI* within the same FRAP experiment (same recording/region) to correct for photobleaching, rather than using the average in one run. Recordings without a suitable P_ROI were excluded from the analysis.

Time	CT2	CT3	CT4	CT5	CT6	CT7	CT8	CT9	CT10
N of included nuclei ($r^2 \geqslant 0.5$)	4	21	20	25	26	36	28	24	16
N of excluded nuclei ($r^2 < 0.5$)	0	0	0	0	1	2	1	2	2

428

429 **Luciferase assay**: All luciferase assays were performed and analyzed in the same way as
430 described previously (Kelliher et al. 2023). Unless otherwise specified, all entrainments and
431 recordings were performed at 25°C. For the benomyl test in Fig. S1D, 50 µl per well of water or
432 2.5 µg/ml benomyl was injected at indicated time using 1ml syringes. All other drugs, as well as
433 the inducer quinic acid, were added directly to the medium before inoculation at the indicated
434 concentrations.

435 **Immunoprecipitation and Western blot**: Co-IP experiments were performed following lab
436 protocol with slight modifications (Chen et al. 2010). Protein samples were collected, and Input
437 samples were saved, using the same method described in Wang et al., (2025). For V5 IP, V5
438 beads were prepared by preincubating 2µl V5 antibody (Invitrogen #46-0705) with 30µl
439 Dynabeads™ Protein G (Invitrogen #1003D) per sample at 4°C for 1 hour. After determining
440 protein concentrations in the protein samples by Bradford assay, 2mg protein per sample in a
441 1ml volume was incubated with the V5 beads at 4°C for 2 hours or overnight. The bound
442 complex was then eluted with 100µl 2x Sample Buffer (Diluted from NuPAGE™ LDS Sample
443 Buffer (4X), Invitrogen #NP0007) following two washes with Wash Buffer (50mM Hepes-KOH,
444 pH 7.4, 150mM NaCl, 0.4% NP-40) and two washes with no-NP Wash Buffer (50mM Hepes-
445 KOH, pH 7.4, 150mM NaCl). For detection, 30µg Input and 10µl IP samples were loaded onto
446 NuPAGE™ 3-8% Tris-Acetate Mini Protein Gels (ThermoFisher Scientific, Catalog
447 #EA03785BOX). Western blotting was then performed as described in Wang et al., (2025).

448 For the *qa_dsimpα* samples, cultures were initiated in 10cm dishes with LCM (no QA). Five
449 ~1cm diameter circles were cut and transferred to 275ml flasks containing 50ml LCM, with or
450 without 10^{-2}M QA (as indicated in figures), and cultured for 21 hours before harvest. For all other
451 samples, strains were maintained in the same LCM medium (with or without 10^{-2}M QA)
452 throughout the culture. All cultures were performed in light at 25°C unless stated otherwise.

453 **Fluorescent imaging**: Samples were grown at 25 °C in the light on agarose pads (1× Vogel's
454 Salts, 2% sucrose, 0.5% arginine, 50 ng/mL biotin, 1% agarose) overnight, unless otherwise
455 specified, and imaged using the 'inverted agar block' method (Hickey et al. 2004) on one of two
456 Nikon Eclipse Ti-E stand-based spinning disk confocal microscope systems described in
457 Chapter 4. 10 µm z-stacks (35 slices at 300 nm step size) were collected in corresponding
458 channels. Tip regions were cropped in ImageJ and then 3D reconstituted in Arivis Vision 4D for
459 segmentation and quantification. Mean fluorescent signals from both the total hyphae and
460 individual nuclei were measured and background signals, defined as the mean intensity from a
461 manually generated object outside the hyphae in each z-stack, were subtracted. The coefficient
462 of variation (CV) for each nucleus was calculated as the standard deviation of its fluorescence

463 signal (SD) divided by its background subtracted mean fluorescent signal
464 ($MEAN_{background\ substracted}$):

465 $$CV = \frac{SD}{MEAN_{background\ substracted}}$$

466 For Fig. 5E, samples were germinated on agarose pads without drug in light and then
467 transferred to darkness for 12 hours. At DD12, a small piece of agarose at the growth front was
468 cut, and its top surface was immersed in water or a 40μM drug solution. After 2 hours of drug
469 and light exposure, samples were imaged using the same methods. Quinic acid was added to
470 the agarose pad prior to inoculation in corresponding experiments.

471 **Race tubes / growth tests**: Race tube assays were performed as described previously
472 (Aronson et al. 1994). or growth tests with Impβ1 inhibitors, race tube medium was
473 supplemented with the indicated concentrations of drug. Conidia of strain 661-4a (*his-3::frq*$_{cbox}$-
474 *luc*) were inoculated at the edge of 35-mm dishes and incubated overnight at 25 °C in constant
475 light before being scanned.

476 **RT-qPCR**: Samples were cultured and harvested as described for Western blotting. RNA was
477 extracted from ~200μg ground powder per sample using Direct-zol RNA Miniprep Kits
478 (ZYMO Research, R2050). For cDNA synthesis, 3μg extracted RNA reverse-transcribed using
479 SuperScript™ IV First-Strand Synthesis System (Invitrogen, 18091050) with the provided Oligo
480 d(T)$_{20}$ primer. The resulting cDNA was diluted to ~7.5 ng/μl, and 2 μl was used for RT-qPCR with
481 iTaq Universal SYBR Green Supermix (Bio-Rad, #1725121) measured with an Applied
482 Biosystems™ StepOne™ Real-Time PCR System. The primers used for RT-qPCR are listed
483 below:

Target	Primers	Product Length	Source
crp-43 NCU08964	Forward: CTGTCCGTACTCGTGACTCC Reverse: ACCATCGATGAGGAGCTTGC	173bp	(Hurley et al. 2015)
Impα NCU01249	Forward: GCATGCTCAGGAATGCTACC Reverse: TCGTCGTCGAGCGAGTAGAC	178bp	This study
wc-1 NCU02356	Forward: TCAGCAGCATCAGTTCAACC Reverse: GTTGATGTTCGCCCATCTCT	116bp	(Chen et al. 2009)
frq NCU02265	Forward: TGGCTCGGATAAGAATGGTC Reverse: ATGAAAGGTGTCCGAAGGTG	103bp	(Chen et al. 2009)

Impβ1 NCU02011	Forward: GGATCCTAACCGCAGCGAAG Reverse: GATCATGGCGGTGATCCAGT	179bp	This study

RT-qPCR data were analyzed using the $\Delta\Delta C_t$ method, with *crp-43* (NCU08964) (Hurley et al. 2015) as the internal control. All reactions were performed in triplicate for each biological sample in one biological replicate, and results are presented as mean ± standard deviation from 3 independent biological replicates.

For light pulse experiments, samples were initiated in light, the cut circles were transferred to flasks in the dark and cultured for 21 h. Cultures were then either harvested in dark (DD21) or exposed to light for 15 minutes before harvest (15min LP).

Statistical analysis and data visualization:

Statistical analysis was performed using Prism 10 (GraphPad) with either one-way ANOVA followed by multiple comparisons or Welch's t test. The number of replicates (n) used for each experiment are indicated in the relevant figure legends. All schematic diagrams were created in BioRender.

DATA AVAILABILITY STATEMENT

The authors affirm that all data necessary for confirming the conclusions of the article are present within the article, figures, and tables. Strains and plasmids are available upon request.

ACKNOWLEDGMENTS

This study was supported by a National Institutes of Health (NIH) grant awarded to Jay C. Dunlap (R35GM118021). We acknowledge use of stocks from the Fungal Genetics Stock Center (FGSC.net), NIAID-supported informatic resources at FungiDB (Contract HHSN75N93019C00077), and Molecular Biology facilities supported by the Dartmouth CQB COBRE (NIH NIGMS grant P20GM130454), and the Dartmouth BioMT (NIH NIGMS grant P20-GM113132). Imaging was performed in the Life Sciences Light Microscopy Facility (RRID:SCR_027143) at Dartmouth College.

REFERENCES

Aronson BD, Johnson KA, Loros JJ, Dunlap JC. 1994. Negative Feedback Defining a Circadian Clock: Autoregulation of the Clock Gene frequency. Science. 263(5153):1578–1584. doi:10.1126/science.8128244.

Baker CL. 2010. Post-translational regulation of the Neurospora crassa circadian system [Ph.D.]. Dartmouth College. [accessed 2025 Sept 14]. https://www.proquest.com/docview/219994612/abstract/9232CEC881334441PQ/1.

Baker CL, Kettenbach AN, Loros JJ, Gerber SA, Dunlap JC. 2009. Quantitative Proteomics Reveals a Dynamic Interactome and Phase-Specific Phosphorylation in the Neurospora Circadian Clock. Mol Cell. 34(3):354–363. doi:10.1016/j.molcel.2009.04.023.

Bartholomai BM. 2022. Cell Biological Dissection of the Neurospora Circadian Oscillator: Tools, Approaches, and Fundamental Observations [Ph.D.]. [United States -- New Hampshire]: Dartmouth College. https://www.proquest.com/dissertations-theses/cell-biological-dissection-neurospora-circadian/docview/2632997349/se-2?accountid=10422.

Beck M, Hurt E. 2017. The nuclear pore complex: understanding its function through structural insight. Nat Rev Mol Cell Biol. 18(2):73–89. doi:10.1038/nrm.2016.147.

Bernardes NE, Fukuda CA, da Silva TD, de Oliveira HC, de Barros AC, Dreyer TR, Bertolini MC, Fontes MRM. 2020. Comparative study of the interactions between fungal transcription factor nuclear localization sequences with mammalian and fungal importin-alpha. Sci Rep. 10(1):1458. doi:10.1038/s41598-020-58316-9.

Bernardes NE, Takeda AAS, Dreyer TR, Freitas FZ, Bertolini MC, Fontes MRM. 2015. Structure of Importin-α from a Filamentous Fungus in Complex with a Classical Nuclear Localization Signal. PLOS ONE. 10(6):e0128687. doi:10.1371/journal.pone.0128687.

Cha J, Chang S, Huang G, Cheng P, Liu Y. 2008. Control of WHITE COLLAR localization by phosphorylation is a critical step in the circadian negative feedback process. EMBO J. 27(24):3246–3255. doi:10.1038/emboj.2008.245.

Chen C-H, DeMay BS, Gladfelter AS, Dunlap JC, Loros JJ. 2010. Physical interaction between VIVID and white collar complex regulates photoadaptation in Neurospora. Proc Natl Acad Sci. 107(38):16715–16720. doi:10.1073/pnas.1011190107.

Chen C-H, Ringelberg CS, Gross RH, Dunlap JC, Loros JJ. 2009. Genome-wide analysis of light-inducible responses reveals hierarchical light signalling in Neurospora. EMBO J. 28(8). doi:10.1038/emboj.2009.54.

Cheng P, Yang Y, Heintzen C, Liu Y. 2001. Coiled-coil domain-mediated FRQ–FRQ interaction is essential for its circadian clock function in Neurospora. EMBO J. 20(1–2):101–108. doi:10.1093/emboj/20.1.101.

Cheng P, Yang Y, Wang L, He Q, Liu Y. 2003. WHITE COLLAR-1, a Multifunctional NeurosporaProtein Involved in the Circadian Feedback Loops, Light Sensing, and Transcription Repression of wc-2 *. J Biol Chem. 278(6):3801–3808. doi:10.1074/jbc.M209592200.

Chook Y, Blobel G. 2001. Karyopherins and nuclear import. Curr Opin Struct Biol. 11(6):703–715. doi:10.1016/S0959-440X(01)00264-0.

Conti E, Uy M, Leighton L, Blobel G, Kuriyan J. 1998. Crystallographic Analysis of the Recognition of a Nuclear Localization Signal by the Nuclear Import Factor Karyopherin α. Cell. 94(2):193–204. doi:10.1016/S0092-8674(00)81419-1.

Costa JI, Muñoz-Guzmán F, Larrondo LF. 2025. Clock Regulation and Fungal Physiology: Molecular Mechanisms Underpinning the Timely Control of Just About Everything. doi:10.1146/annurev-micro-060424-051158. [accessed 2025 Aug 9]. https://www.annualreviews.org/content/journals/10.1146/annurev-micro-060424-051158.

Crosthwaite SK, Dunlap JC, Loros JJ. 1997. Neurospora wc-1 and wc-2: Transcription, Photoresponses, and the Origins of Circadian Rhythmicity. Science. 276(5313):763–769. doi:10.1126/science.276.5313.763.

Dasgupta A. 2015. Biological Significance of VIVID Photocycle Length and the Control of Gene Expression by the Neurospora Clock [Ph.D.]. Dartmouth College. [accessed 2025 Sept 15]. https://www.proquest.com/docview/1758936730/abstract/29396917764B407CPQ/1.

Dekhang R, Wu C, Smith KM, Lamb TM, Peterson M, Bredeweg EL, Ibarra O, Emerson JM, Karunarathna N, Lyubetskaya A, et al. 2017. The Neurospora Transcription Factor ADV-1 Transduces Light Signals and Temporal Information to Control Rhythmic Expression of Genes Involved in Cell Fusion. G3 GenesGenomesGenetics. 7(1):129–142. doi:10.1534/g3.116.034298.

Denault DL, Loros JJ, Dunlap JC. 2001. WC-2 mediates WC-1–FRQ interaction within the PAS protein-linked circadian feedback loop of Neurospora. EMBO J. 20(1–2):109–117. doi:10.1093/emboj/20.1.109.

Dunlap JC. 1999. Molecular Bases for Circadian Clocks. Cell. 96(2):271–290. doi:10.1016/S0092-8674(00)80566-8.

Dunlap JC, Loros JJ. 2017. Making Time: Conservation of Biological Clocks from Fungi to Animals. Microbiol Spectr. 5(3):10.1128/microbiolspec.funk-0039–2016. doi:10.1128/microbiolspec.funk-0039-2016.

Galagan JE, Calvo SE, Borkovich KA, Selker EU, Read NO, Jaffe D, FitzHugh W, Ma LJ, Smirnov S, Purcell S, et al. 2003. The genome sequence of the filamentous fungus Neurospora crassa. Nat 2003 4226934. 422(6934):859–868. doi:10.1038/nature01554.

Giles NH, Case ME, Baum J, Geever R, Huiet L, Patel V, Tyler B. 1985. Gene organization and regulation in the qa (quinic acid) gene cluster of Neurospora crassa. Microbiol Rev. 49(3):338–358. doi:10.1128/mr.49.3.338-358.1985.

Goldfarb DS, Corbett AH, Mason DA, Harreman MT, Adam SA. 2004. Importin α: a multipurpose nuclear-transport receptor. Trends Cell Biol. 14(9):505–514. doi:10.1016/j.tcb.2004.07.016.

Haruki H, Nishikawa J, Laemmli UK. 2008. The Anchor-Away Technique: Rapid, Conditional Establishment of Yeast Mutant Phenotypes. Mol Cell. 31(6):925–932. doi:10.1016/j.molcel.2008.07.020.

He L, Guo W, Li J, Meng Y, Wang Y, Lou H, He Q. 2020. Two dominant selectable markers for genetic manipulation in Neurospora crassa. Curr Genet. 66(4):835–847. doi:10.1007/s00294-020-01063-1.

Hickey PC, Swift SR, Roca MG, Read ND. 2004. Live-cell Imaging of Filamentous Fungi Using Vital Fluorescent Dyes and Confocal Microscopy. In: Methods in Microbiology. Vol. 34. Academic Press. (Microbial Imaging). p. 63–87. [accessed 2025 July 5]. https://www.sciencedirect.com/science/article/pii/S0580951704340031.

Hurley JH, Dasgupta A, Andrews P, Crowell AM, Ringelberg C, Loros JJ, Dunlap JC. 2015. A Tool Set for the Genome-Wide Analysis of Neurospora crassa by RT-PCR. G3-GENES GENOMES Genet. 5(10):2043–2049. doi:10.1534/g3.115.019141.

Jang AR, Moravcevic K, Saez L, Young MW, Sehgal A. 2015. Drosophila TIM Binds Importin α1, and Acts as an Adapter to Transport PER to the Nucleus. PLOS Genet. 11(2):e1004974. doi:10.1371/JOURNAL.PGEN.1004974.

Káldi K, González BH, Brunner M. 2006. Transcriptional regulation of the Neurospora circadian clock gene wc-1 affects the phase of circadian output. EMBO Rep. 7(2):199–204. doi:10.1038/sj.embor.7400595.

Kelliher CM, Stevenson E-L, Loros JJ, Dunlap JC. 2023. Nutritional compensation of the circadian clock is a conserved process influenced by gene expression regulation and mRNA stability. PLOS Biol. 21(1):e3001961. doi:10.1371/journal.pbio.3001961.

Klocko AD, Rountree MR, Grisafi PL, Hays SM, Adhvaryu KK, Selker EU. 2015. Neurospora Importin α Is Required for Normal Heterochromatic Formation and DNA Methylation. PLOS Genet. 11(3):e1005083. doi:10.1371/journal.pgen.1005083.

Korge S, Maier B, Brüning F, Ehrhardt L, Korte T, Mann M, Herrmann A, Robles MS, Kramer A. 2018. The non-classical nuclear import carrier Transportin 1 modulates circadian rhythms through its effect on PER1 nuclear localization. PLoS Genet. 14:e1007189. doi:10.1371/journal.pgen.1007189.

616 Kwon I, Lee J, Chang SH, Jung NC, Lee BJ, Son GH, Kim K, Lee KH. 2006. BMAL1 Shuttling
617 Controls Transactivation and Degradation of the CLOCK/BMAL1 Heterodimer. Mol Cell Biol.
618 26(19):7318–7330. doi:10.1128/MCB.00337-06.

619 Larrondo LF, Colot HV, Baker CL, Loros JJ, Dunlap JC. 2009. Fungal Functional Genomics:
620 Tunable Knockout-Knock-in Expression and Tagging Strategies. Eukaryot Cell. 8(5):800–
621 804. doi:10.1128/ec.00072-09.

622 Lauinger L, Diernfellner A, Falk S, Brunner M. 2014. The RNA helicase FRH is an ATP-
623 dependent regulator of CK1a in the circadian clock of Neurospora crassa. Nat Commun.
624 5(1):3598. doi:10.1038/ncomms4598.

625 Lee K, Dunlap JC, Loros JJ. 2003. Roles for WHITE COLLAR-1 in Circadian and General
626 Photoperception in *Neurospora crassa*. Genetics. 163(1). doi:10.1093/genetics/163.1.103.

627 Lee Y, Jang AR, Francey LJ, Sehgal A, Hogenesch JB. 2015. KPNB1 mediates PER/CRY
628 nuclear translocation and circadian clock function. Kramer A, editor. eLife. 4:e08647.
629 doi:10.7554/eLife.08647.

630 Lee Y, Shen Y, Francey LJ, Ramanathan C, Sehgal A, Liu AC, Hogenesch JB. 2019. the nRon
631 complex controls circadian clock function through regulated peR and cRY nuclear
632 translocation. Sci Rep 2019 91. 9(1):1–12. doi:10.1038/s41598-019-48341-8.

633 Lin C, Feng S, DeOliveira CC, Crane BR. 2023. Cryptochrome–Timeless structure reveals
634 circadian clock timing mechanisms. Nature. 617(7959):194–199. doi:10.1038/s41586-023-
635 06009-4.

636 Luo C, Loros JJ, Dunlap JC. 1998. Nuclear localization is required for function of the
637 essential clock protein FRQ. EMBO J. 17(5):1228–1235. doi:10.1093/emboj/17.5.1228.

638 Mans B, Anantharaman V, Aravind L, Koonin EV. 2004. Comparative Genomics, Evolution
639 and Origins of the Nuclear Envelope and Nuclear Pore Complex. Cell Cycle. 3(12):1625–
640 1650. doi:10.4161/cc.3.12.1316.

641 Markina-Iñarrairaegui A, Etxebeste O, Herrero-García E, Araújo-Bazán L, Fernández-
642 Martínez J, Flores JA, Osmani SA, Espeso EA. 2011. Nuclear transporters in a
643 multinucleated organism: functional and localization analyses in Aspergillus nidulans. Mol
644 Biol Cell. 22(20):3874–3886. doi:10.1091/mbc.e11-03-0262.

645 Mason DA, Stage DE, Goldfarb DS. 2009. Evolution of the Metazoan-Specific Importin α
646 Gene Family. J Mol Evol. 68(4):351–365. doi:10.1007/s00239-009-9215-8.

647 Metzenberg R. 2004. Bird Medium: an alternative to Vogel Medium. Fungal Genet Rep.
648 51(1):19–20. doi:10.4148/1941-4765.1138.

Öllinger R, Korge S, Korte T, Koller B, Herrmann A, Kramer A. 2014. Dynamics of the circadian clock protein PERIOD2 in living cells. J Cell Sci. 127(19):4322–4328. doi:10.1242/jcs.156612.

Pelham JF, Mosier AE, Altshuler SC, Rhodes ML, Kirchhoff CL, Fall WB, Mann C, Baik LS, Chiu JC, Hurley JM. 2023. Conformational changes in the negative arm of the circadian clock correlate with dynamic interactomes involved in post-transcriptional regulation. Cell Rep. 42(4). doi:10.1016/j.celrep.2023.112376. [accessed 2025 July 7]. https://www.cell.com/cell-reports/abstract/S2211-1247(23)00387-X.

Pemberton LF, Paschal BM. 2005. Mechanisms of Receptor-Mediated Nuclear Import and Nuclear Export. Traffic. 6(3):187–198. doi:10.1111/j.1600-0854.2005.00270.x.

Saez L, Derasmo M, Meyer P, Stieglitz J, Young MW. 2011. A Key Temporal Delay in the Circadian Cycle of Drosophila Is Mediated by a Nuclear Localization Signal in the Timeless Protein. Genetics. 188(3):591–600. doi:10.1534/genetics.111.127225.

Sakakida Y, Miyamoto Y, Nagoshi E, Akashi M, Nakamura TJ, Mamine T, Kasahara M, Minami Y, Yoneda Y, Takumi T. 2005. Importin α/β mediates nuclear transport of a mammalian circadian clock component, mCRY2, together with mPER2, through a bipartite nuclear localization signal. J Biol Chem. 280(14):13272–13278. doi:10.1074/jbc.M413236200.

Schafmeier T, Diernfellner A, Schäfer A, Dintsis O, Neiss A, Brunner M. 2008. Circadian activity and abundance rhythms of the Neurospora clock transcription factor WCC associated with rapid nucleo–cytoplasmic shuttling. Genes Dev. 22(24):3397–3402. doi:10.1101/gad.507408.

Schunke C, Ruppert B, Schultz S, Diernfellner ACR, Brunner M. 2025. CK1a-Mediated Two-Step Subunit Remodeling of the Circadian FRQ-FRH Complex. :2025.05.13.653691. doi:10.1101/2025.05.13.653691. [accessed 2025 Aug 4]. https://www.biorxiv.org/content/10.1101/2025.05.13.653691v1.

Schwerdtfeger C, Linden H. 2000. Localization and light-dependent phosphorylation of white collar 1 and 2, the two central components of blue light signaling in Neurospora crassa. Eur J Biochem. 267(2):414–422. doi:10.1046/j.1432-1327.2000.01016.x.

Shi M, Collett M, Loros JJ, Dunlap JC. 2010. FRQ-Interacting RNA Helicase Mediates Negative and Positive Feedback in the Neurospora Circadian Clock. Genetics. 184(2):351–361. doi:10.1534/genetics.109.111393.

Smith KM, Sancar G, Dekhang R, Sullivan CM, Li S, Tag AG, Sancar C, Bredeweg EL, Priest HD, McCormick RF, et al. 2010. Transcription Factors in Light and Circadian Clock Signaling Networks Revealed by Genomewide Mapping of Direct Targets for Neurospora White Collar Complex. Eukaryot Cell. 9(10):1549–1556. doi:10.1128/ec.00154-10.

Smyllie NJ, Pilorz V, Boyd J, Meng Q-J, Saer B, Chesham JE, Maywood ES, Krogager TP, Spiller DG, Boot-Handford R, et al. 2016. Visualizing and Quantifying Intracellular Behavior and Abundance of the Core Circadian Clock Protein PERIOD2. Curr Biol. 26(14):1880–1886. doi:10.1016/j.cub.2016.05.018.

Soderholm JF, Bird SL, Kalab P, Sampathkumar Y, Hasegawa K, Uehara-Bingen M, Weis K, Heald R. 2011. Importazole, a Small Molecule Inhibitor of the Transport Receptor Importin-β. ACS Chem Biol. 6(7):700–708. doi:10.1021/cb2000296.

Ström A-C, Weis K. 2001. Importin-beta-like nuclear transport receptors. Genome Biol. 2(6):reviews3008.1. doi:10.1186/gb-2001-2-6-reviews3008.

Takeda AAS, Freitas FZ, Magro AJ, Bernardes NE, Fernandes CAH, Goncalves RD, Bertolini MC, Fontes MRM. 2013. Biophysical Characterization of the Recombinant Importin-α from Neurospora crassa. http://www.eurekaselect.com. [accessed 2025 Sept 16]. https://www.eurekaselect.com/article/47441.

Umemura Y, Koike N, Matsumoto T, Yoo S-H, Chen Z, Yasuhara N, Takahashi JS, Yagita K. 2014. Transcriptional program of Kpna2/Importin-α2 regulates cellular differentiation-coupled circadian clock development in mammalian cells. Proc Natl Acad Sci. 111(47):E5039–E5048. doi:10.1073/pnas.1419272111.

Wagstaff KM, Rawlinson SM, Hearps AC, Jans DA. 2011. An AlphaScreen®-Based Assay for High-Throughput Screening for Specific Inhibitors of Nuclear Import. J Biomol Screen. 16(2):192–200. doi:10.1177/1087057110390360.

Wang B, Zhou X, Loros JJ, Dunlap JC. 2016. Alternative Use of DNA Binding Domains by the Neurospora White Collar Complex Dictates Circadian Regulation and Light Responses. Mol Cell Biol. 36(5):781–793. doi:10.1128/MCB.00841-15.

Wang Z, Bartholomai BM, Wang B, Ritz D, Schultz D, Loros JJ, Dunlap JC. 2025. Core Clock Protein Subcellular Dynamics Coordinate Local and Global Circadian Control in Syncytia. :2025.09.30.679467. doi:10.1101/2025.09.30.679467. [accessed 2025 Nov 17]. https://www.biorxiv.org/content/10.1101/2025.09.30.679467v1.

713 **FIGURE LEGENDS**

714 **Figure 1 | Nuclear import of FRQ is circadian regulated.**

715 A) Schematic of the experimental design. FRAP experiments were performed during the
716 subjective day following entrainment by temperature cycles. Whole nuclei were bleached, and
717 the recovery of their fluorescent signal reflects nuclear import of cytoplasmic FRQ. B) Example
718 timelapses from subjective morning (CT4, top) and afternoon (CT8, bottom), showing different
719 recovery rates`. White arrowheads indicate example target nuclei. Scale bar = 5 μm. C) Average
720 fluorescent recovery curves for each hour of the subjective day. D) Nuclear signal recovery
721 speed, calculated as the slope of linear regression of each target nucleus's recovery curve.
722 Data were analyzed by Pearson correlation, with the correlation coefficient (r) and p-value
723 indicated in the plot.

724 **Figure 2 | Core clock proteins directly bind Importinα while bypassing the classic NLS for**
725 **nuclear import.**

726 A) Co-immunoprecipitation between endogenous Importinα and core clock proteins. Cell lysates
727 were immunoprecipitated with anti-V5 antibody. The interaction between FRQ and FRH is
728 included as a positive control. B) Example central focal images showing FRQ or $FRQ^{\Delta NLS}$
729 subcellular localization during free-run circadian cycles or in constant light. FRQ is shown in
730 green, the inner nuclear envelope marker NUP211 in blue, and the outer nuclear envelope
731 marker NUP159 in magenta. All targets are endogenously tagged with monomeric fluorescent
732 proteins. Scale bar = 10 μm. C) Quantification of nuclear FRQ or $FRQ^{\Delta NLS}$ signal from 3D
733 renderings of z-stacks (Mean ± SD). Each dot represents the mean fluorescent signal of one
734 nucleus. N = 7-11 hyphal tips per condition, with the ungrouped data of each tip plotted in Fig.
735 S2E.

736 **Figure 3 | Impα is required for normal circadian rhythmicity.**

737 A) Schematic of the siRNA knockdown design. Expression of dsDNA targeting the last exon of
738 *impα* is driven by the *qa-2* inducible promoter. With the addition of the inducer quinic acid (QA),
739 dsRNA is expressed and subsequently processed to inhibit *impα* expression. B) Growth of
740 *qa_dsimpα* strains in race tubes with or without 10^{-2} M QA. C) Expression level of *impα* (top),
741 *wc-1* (middle), or *frq* (bottom) in control ($impα^{V5}$) or *qa_dsimpα* strains with or without 10^{-2} M QA
742 quantified by RT-qPCR. Error bars represent the standard deviation from biological triplicates.
743 D) Protein levels in control ($impα^{V5}$) or *qa_dsimpa* strains with or without 10^{-2} M QA. Example
744 targets, including core clock proteins, were detected by immunoblotting (left), and total protein
745 levels were assessed by Coomassie staining (right). * indicates unspecific bands in
746 immunoblots. E) Luciferase assays of control ($impα^{V5}$) or *qa_dsimpα* strains with varying QA
747 concentrations (top) and corresponding period lengths (bottom). n=4 replicates per condition.
748 Error bars show one standard deviation. Periods were analyzed by one-way ANOVA with
749 multiple comparisons.

750

751

Figure 4 | Nuclear localization of FRQ and WC-1, but not WC-2, depends on Impα.

A) Maximum projection images of example z-stacks showing FRQ and WC-2 subcellular localization in constant light with or without 10^{-2} M QA. Scale bar = 10 μm. B-C) Quantification of B) nuclear FRQ or C) total FRQ signal in tip regions from 3D renderings of z-stacks. One control strain (1984-4, *frq*^{mNeonGreen}*::hph+ nup159*^{mTagBFP2}*::nat-1+*) and 2 *csr-1::qa_dsimpα nup159*^{BFP} *wc-2*^{mApple}*; frq*^{mNG} strains were analyzed. 2 (controls) or 3 (*dsimpα* strains) biological replicates were quantified, with individual replicates plotted in Fig. S3B. N = 5-12 hyphal tips per condition per replicate. Each dot represents the mean fluorescent signal of one nucleus (nuclear signal) or one hypha (total signal). D) Schematic of the potential mechanism by which WCC amount and localization are affected when Impα is deficient. E-G) Expression level of E) *wc-1*, F) *frq*, or G) *impα* in a *qa_dsimpα* strain at DD21 with or without 10^{-2} M QA, before or after 15-minute light pulse, quantified by RT-qPCR. Error bars represent the standard deviation from biological triplicates. H-I) Quantification of H) nuclear WC-2 or I) total WC-2 signal in tip regions from 3D renderings of z-stacks. One control strain (1996-2, *wc-2*^{mApple}*::hph+, his-3::cbox-luc*) and 2 *csr-1::qa_dsimpa nup159*^{BFP} *wc-2*^{mApple}*; frq*^{mNG} strains were analyzed. Same methods as Fig. 4B-C were used.

Figure 5 | Deficiency of Importinβs affects FRQ localization or circadian clock.

A) Maximum projection images of example z-stacks showing FRQ subcellular localization with or without Importazole, an Importinβ1 inhibitor. Samples were treated with drug (or water) and light for 2 hours starting at DD12. N = 5-6 hyphal tips. Each dot represents the mean fluorescent signal of one nucleus (nuclear signal) or one hypha (total signal). Scale bar = 10 μm. B-C) Quantification of B) nuclear FRQ or C) total FRQ signal in tip regions from 3D renderings of z-stacks (Mean ± SD). Each dot represents the mean fluorescent signal of one nucleus (nuclear signal) or one hypha (total signal). D) Luciferase assays of control strain (*csr-1::frq*$_{cbox}$*-luc*) or three *Δimpβ2* strains (left) and their period lengths (right). n=4 replicates. The shade shows one standard deviation. Periods were analyzed by one-way ANOVA with multiple comparisons. D) Luciferase assays showing the free-run clock of *Δimpβ2* FRQ imaging strain used in E) compared to its control strain (2066-4) without *Δimpβ2*. Each curve represents the average of three biological triplicates each with 4 technical replicates, with the shade showing one standard deviation. F-G) Maximum projection images of example z-stacks showing F) FRQ or G) WC-1 subcellular localization ((left) and quantification of nuclear signal (right) in constant light, with or without Impβ2. Scale bar = 10 μm. N = 3-6 hyphal tips. Each dot represents the mean fluorescent signal of one nucleus. H) Nuclear FRQ signal recovery speed at CT4 with or without Impβ2, calculated as the slope of linear regression of each target nucleus's recovery curve.

Figure 6 | Shortened period in Impβ3-deficient strains is independent of core clock protein levels or localization.

A) Schematic of the inducible *impβ3* design. Expression of *impβ3* is driven by the *qa-2* inducible promoter. Without the addition of the inducer quinic acid (QA), expression of *impβ3* is reduced. B) Core clock protein levels in control strain or inducible *impβ3* strains with or without 10^{-2} M QA. The result shown is representative of biological triplicates; additional replicates are shown in Fig. S5D. C) Luciferase assays of the inducible *impβ3* strain with varying QA concentrations

793 (left) and their period lengths (right). n=4 replicates. The shade shows one standard deviation.
794 Periods were analyzed by one-way ANOVA with multiple comparisons. D-E) Maximum
795 projection images of example z-stacks showing D) FRQ or E) WC-2 subcellular localization
796 ((left) and quantification of nuclear signal (right) in constant light, with or without 10^{-2} M QA.
797 Scale bar = 10 μm. N = 4-7 hyphal tips. Each dot represents the mean fluorescent signal of one
798 nucleus. Two sibling strains were quantified for WC-2. F) Luciferase assays of strains with both
799 *pph4* deletion and *impβ3* deficiency compared to strains with *impβ3 deficiency* alone. n=4
800 replicates. The shade shows one standard deviation.

801

Figure 1

a

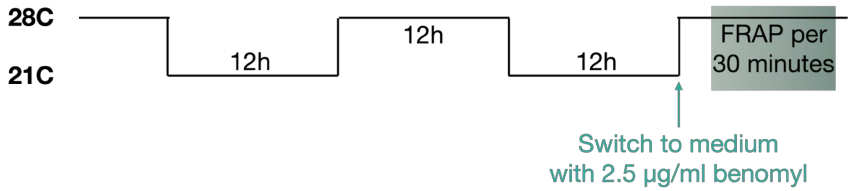

b

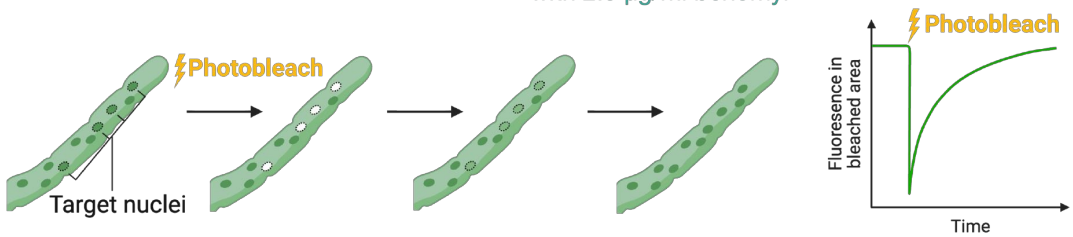

c

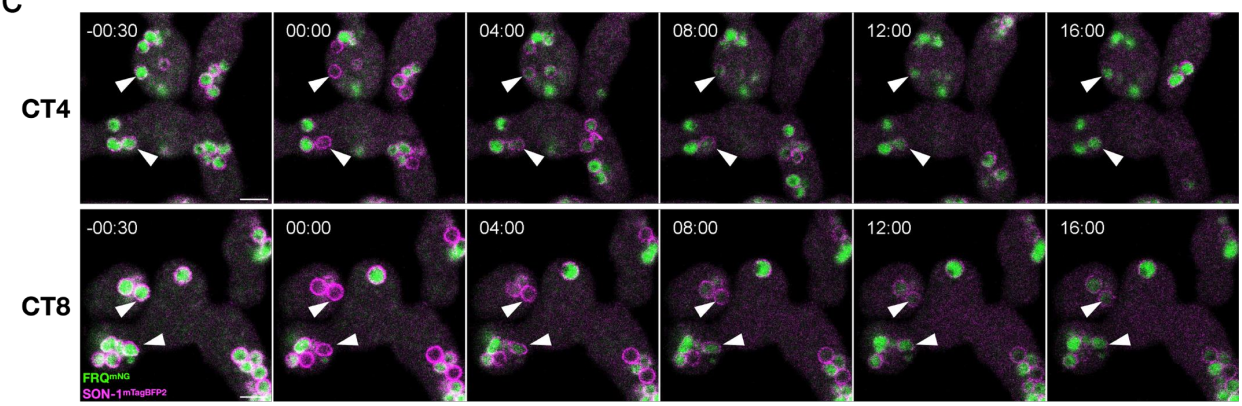

d

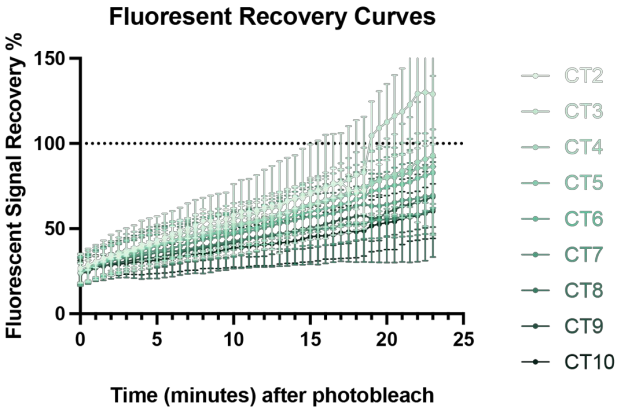

e

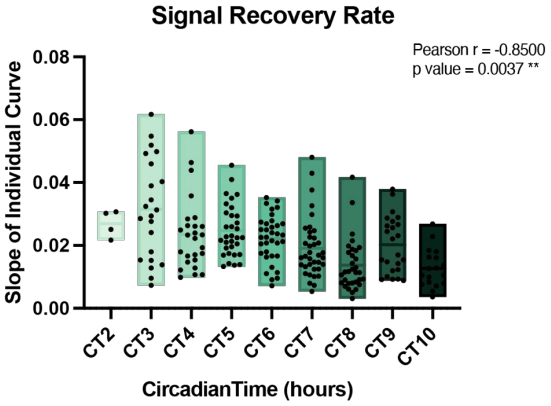

Figure 2

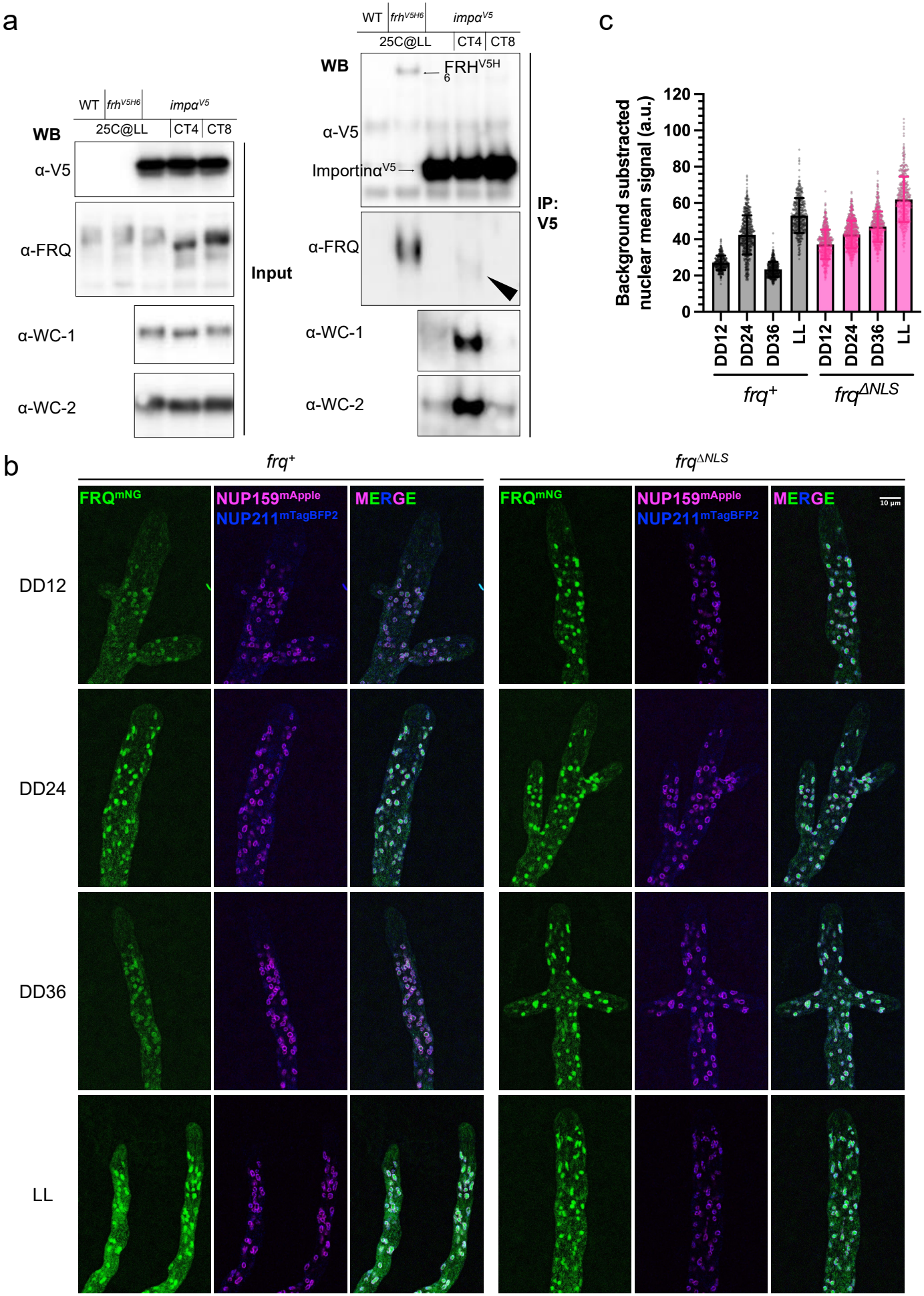
a
WT
frh V5H6
impα V5
25C@LL
CT4
CT8
WB
α-V5
α-FRQ
α-WC-1
α-WC-2
Input
FRH V5H 6
Importinα V5
IP: V5
c
Background substracted nuclear mean signal (a.u.)
120
100
80
60
40
20
0
DD12
DD24
DD36
LL
frq+
frqΔNLS
b
frq+
frqΔNLS
FRQmNG
NUP159mApple
NUP211mTagBFP2
MERGE
10 µm
DD12
DD24
DD36
LL

Figure 3

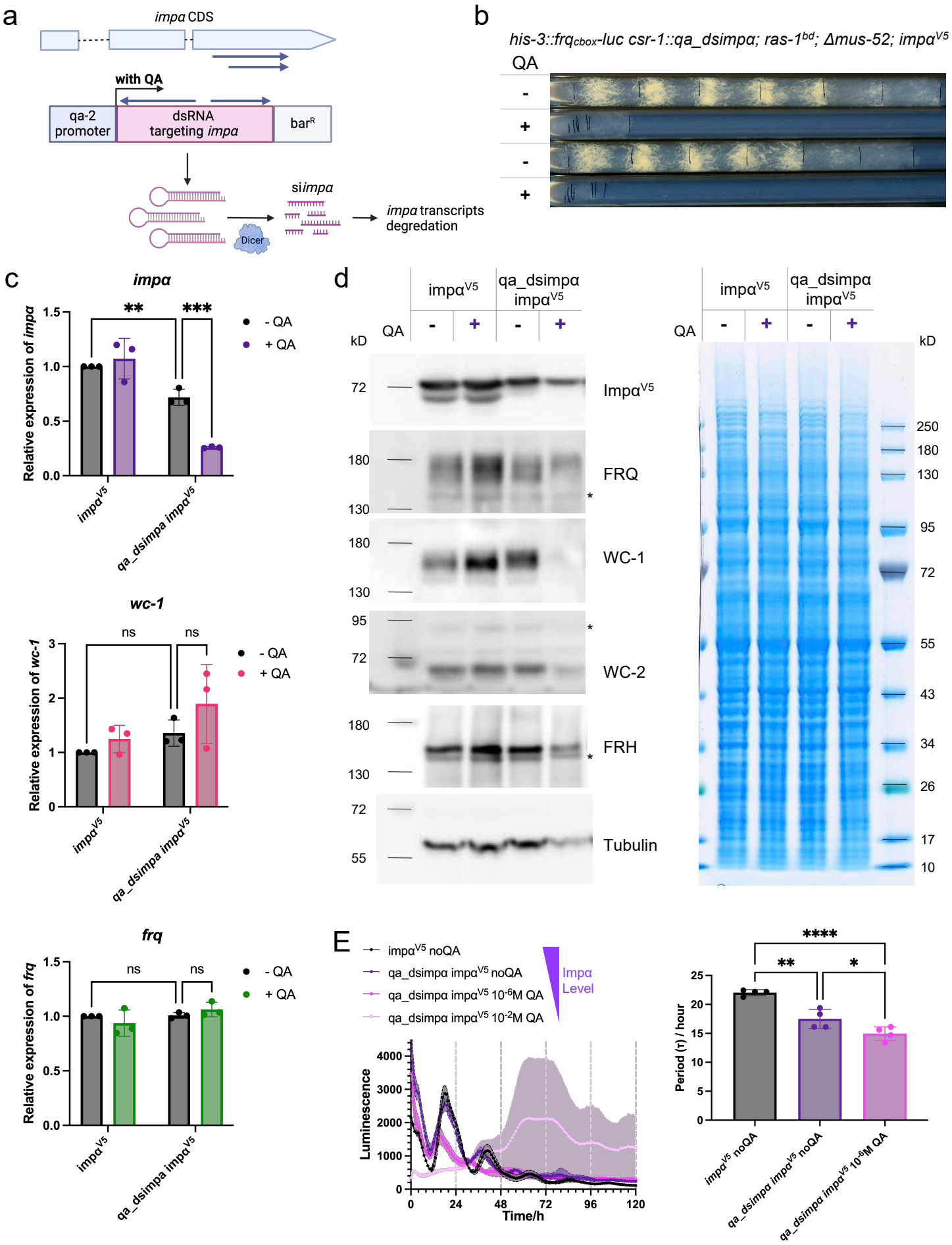
a
impa CDS
with QA
qa-2 promoter
dsRNA targeting impa
barR
siimpa
Dicer
impa transcripts degredation
b
his-3::frqcbox-luc csr-1::qa_dsimpα; ras-1bd; Δmus-52; impaV5
QA
-
+
-
+
c
impa
Relative expression of impa
- QA
+ QA
impaV5
qa_dsimpa impaV5
wc-1
Relative expression of wc-1
ns
frq
Relative expression of frq
d
impaV5
qa_dsimpa impaV5
QA
kD
ImpaV5
FRQ
WC-1
WC-2
FRH
Tubulin
E
impaV5 noQA
qa_dsimpa impaV5 noQA
qa_dsimpa impaV5 10-6M QA
qa_dsimpa impaV5 10-2M QA
Impa Level
Luminescence
Time/h
Period (τ) / hour
impaV5 noQA
qa_dsimpa impaV5 noQA
qa_dsimpa impaV5 10-6M QA

Figure 4

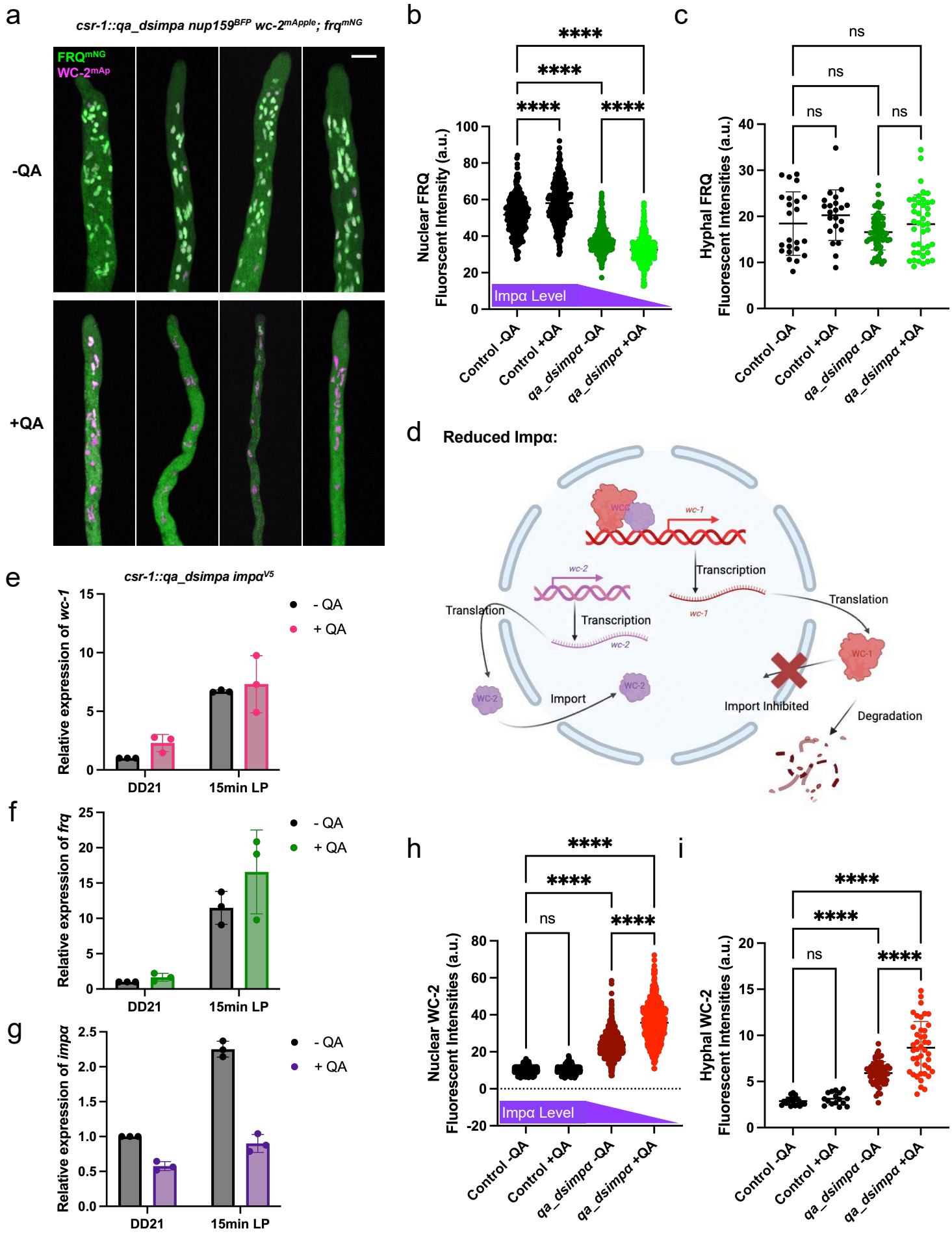
a
csr-1::qa_dsimpa nup159BFP wc-2mApple; frqmNG
FRQmNG
WC-2mAp
-QA
+QA
b
Nuclear FRQ Fluorescent Intensity (a.u.)
Impα Level
Control -QA
Control +QA
qa_dsimpα -QA
qa_dsimpα +QA
c
Hyphal FRQ Fluorescent Intensities (a.u.)
ns
d
Reduced Impα:
WCC
wc-1
wc-2
Transcription
Translation
Import
Import Inhibited
Degradation
WC-1
WC-2
e
csr-1::qa_dsimpa impaV5
Relative expression of wc-1
- QA
+ QA
DD21
15min LP
f
Relative expression of frq
g
Relative expression of impα
h
Nuclear WC-2 Fluorescent Intensities (a.u.)
i
Hyphal WC-2 Fluorescent Intensities (a.u.)

Figure 5

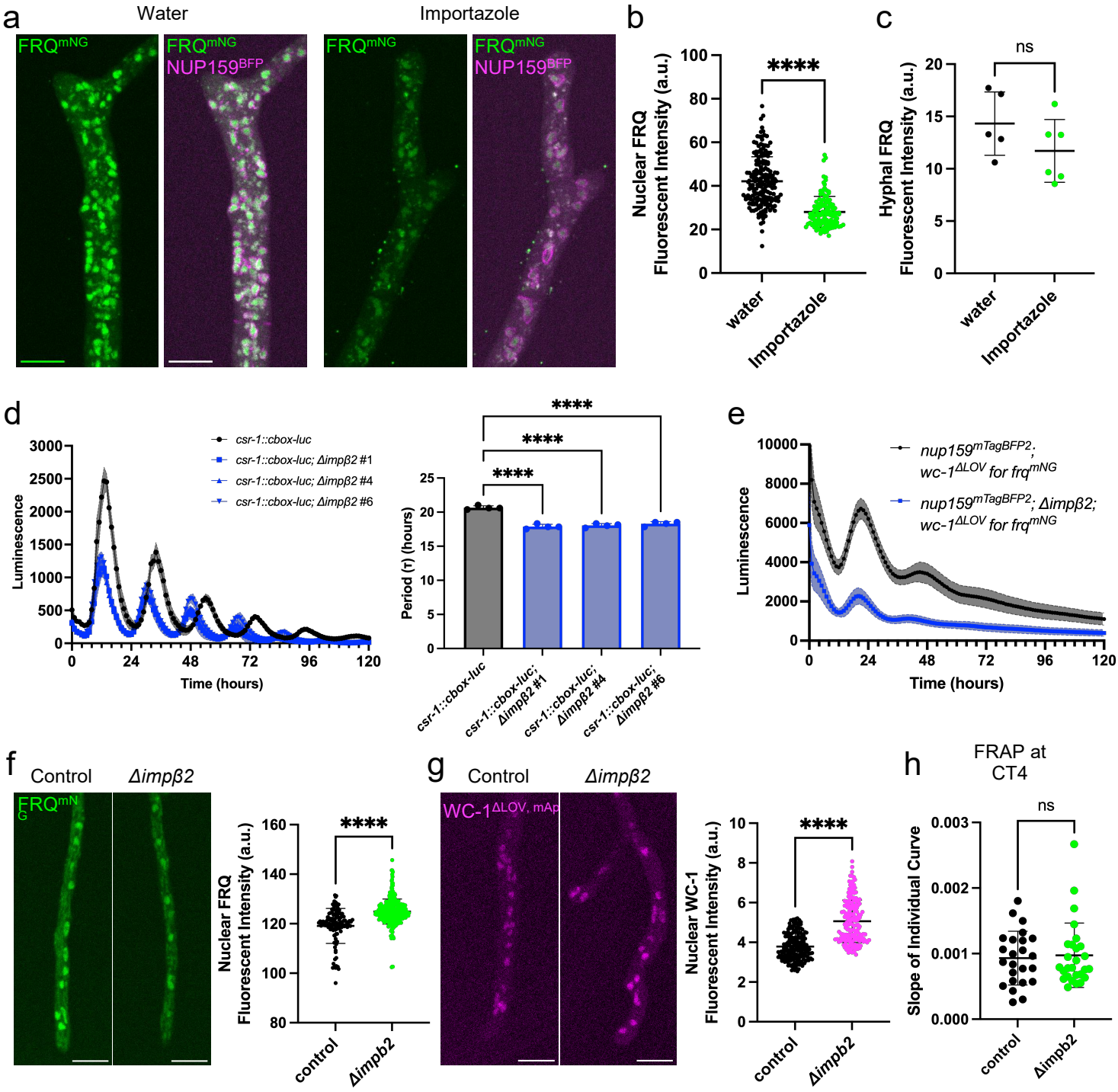
a
Water
Importazole
FRQmNG
FRQmNG
NUP159BFP
FRQmNG
FRQmNG
NUP159BFP
b
Nuclear FRQ Fluorescent Intensity (a.u.)
****
water
Importazole
c
Hyphal FRQ Fluorescent Intensity (a.u.)
ns
water
Importazole
d
Luminescence
Time (hours)
csr-1::cbox-luc
csr-1::cbox-luc; Δimpβ2 #1
csr-1::cbox-luc; Δimpβ2 #4
csr-1::cbox-luc; Δimpβ2 #6
Period (τ) (hours)
****
****
****
csr-1::cbox-luc
csr-1::cbox-luc; Δimpβ2 #1
csr-1::cbox-luc; Δimpβ2 #4
csr-1::cbox-luc; Δimpβ2 #6
e
Luminescence
Time (hours)
nup159mTagBFP2; wc-1ΔLOV for frqmNG
nup159mTagBFP2; Δimpβ2; wc-1ΔLOV for frqmNG
f
Control
Δimpβ2
FRQmNG
Nuclear FRQ Fluorescent Intensity (a.u.)
****
control
Δimpb2
g
Control
Δimpβ2
WC-1ΔLOV, mAp
Nuclear WC-1 Fluorescent Intensity (a.u.)
****
control
Δimpb2
h
FRAP at CT4
Slope of Individual Curve
ns
control
Δimpb2

Figure 6

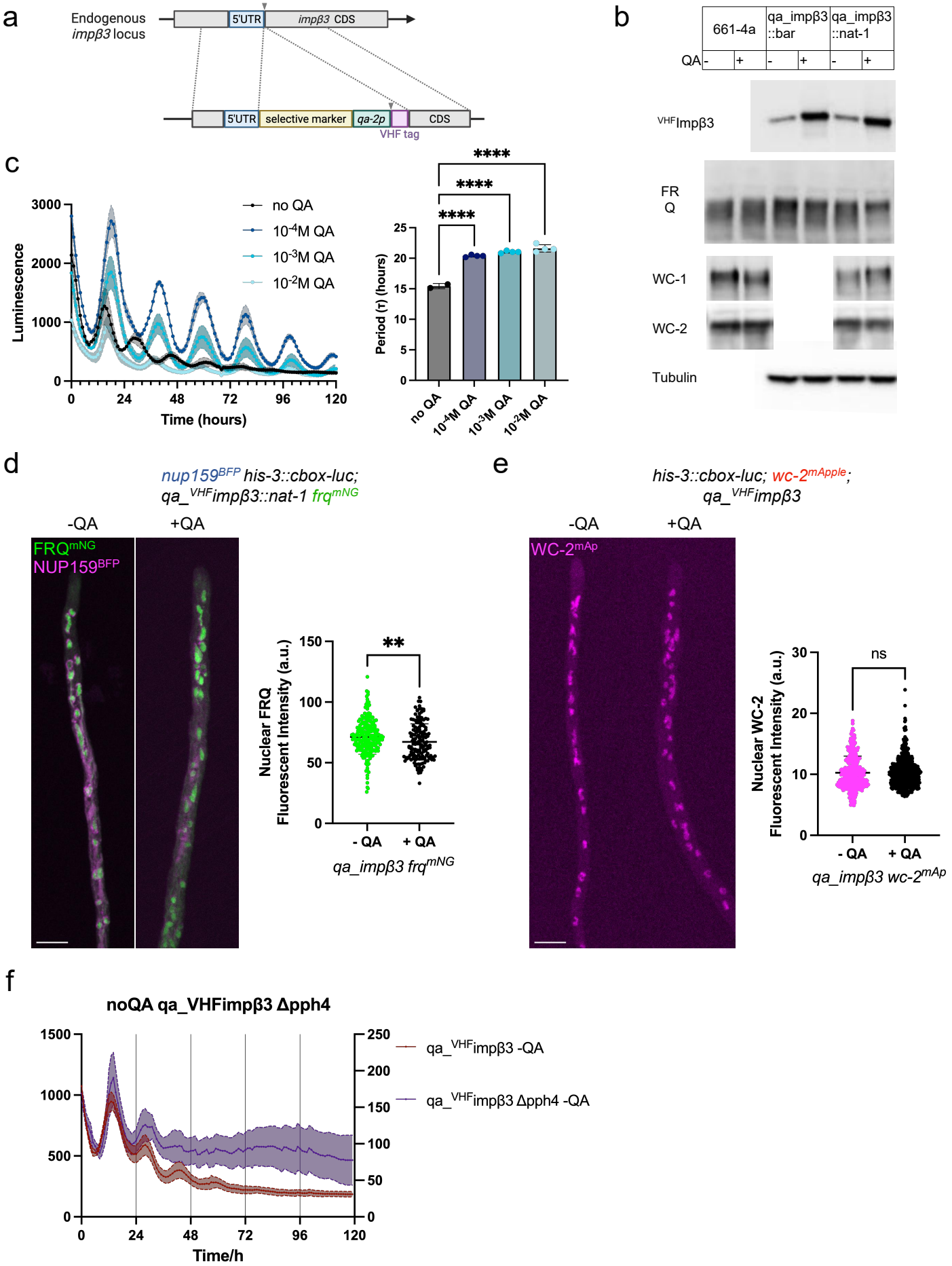
a
Endogenous impβ3 locus
5'UTR
impβ3 CDS
5'UTR
selective marker
qa-2p
CDS
VHF tag
b
661-4a
qa_impβ3 ::bar
qa_impβ3 ::nat-1
QA
VHFImpβ3
FRQ
WC-1
WC-2
Tubulin
c
no QA
10-4M QA
10-3M QA
10-2M QA
Luminescence
Time (hours)
Period (τ) (hours)
****
d
nup159BFP his-3::cbox-luc; qa_VHFimpβ3::nat-1 frqmNG
-QA
+QA
FRQmNG
NUP159BFP
Nuclear FRQ Fluorescent Intensity (a.u.)
**
- QA
+ QA
qa_impβ3 frqmNG
e
his-3::cbox-luc; wc-2mApple; qa_VHFimpβ3
-QA
+QA
WC-2mAp
Nuclear WC-2 Fluorescent Intensity (a.u.)
ns
- QA
+ QA
qa_impβ3 wc-2mAp
f
noQA qa_VHFimpβ3 Δpph4
qa_VHFimpβ3 -QA
qa_VHFimpβ3 Δpph4 -QA
Time/h